Chapter 23

A New Frontier of Photocatalysis Employing Micro-Sized TiO_2: Air/Water Pollution Abatement and Self-Cleaning/Antibacterial Applications

Claudia L. Bianchi, Carlo Pirola, Marta Stucchi, Benedetta Sacchi, Giuseppina Cerrato, Sara Morandi, Alessandro Di Michele, Alessandra Carletti and Valentino Capucci

Additional information is available at the end of the chapter

http://dx.doi.org/10.5772/62892

Abstract

This chapter presents the use of a commercial micro-sized TiO_2 powder as an alternative to the traditional nano-powders as semiconductors in photocatalytic processes. Results of the photocatalytic efficiency towards the photodegradation of the traditional pollutant molecules both in gas phase (nitrogen oxides (NO_x) and volatile organic compounds (VOCs)) and in water phase (phenol) are presented and compared to the results obtained with two nano-sized reference powders. Micro-sized TiO_2 is also industrially coated at the surfaces of porcelain grés tiles (Active Clean Air and Antibacterial Ceramic™). The possibility to have a photocatalytic material, strongly stuck at the surface of a vitrified tile, increases the use of photocatalysis in real conditions: no problem of filtration of the semiconductor from the liquid medium after use and no risks of leakage of nanoparticles in the atmosphere. Tests were performed using reactors equipped with UV-A lamps and with suitable analytical systems, depending on the final purpose. Characterization data from both powders and coated tiles are put in correlation with the photocatalytic results to understand the semiconductor action during the photocatalytic process. Polluting molecules were chosen in order to cover all the common aspects of environmental pollution: NO_x and some VOCs represent the model molecules to test the efficiency of the micro-sized TiO_2 (degradation from the pristine molecule to CO_2 or inorganic salts) in gas phase. As for the water pollution, phenol was chosen as common pollutant in worldwide rivers. Moreover, tests on self-cleaning and antibacterial properties are also reported. The positive results of micro-sized TiO_2 both in powder and coated onto the surface of porcelain grés tiles open the way to new photocatalytic products that do

not make use of nanoscale powders avoiding problems to human safety caused by the inherent toxicity of the nanoparticles.

Keywords: Microsized TiO_2, powder, photocatalytic tiles, NO_x, VOCs, phenol, self-cleaning, oleic acid, *Escherichia coli*, *Staphylococcus aureus*, methicillin-resistant *MRSA*

1. Introduction

The importance of photocatalysis is related to the increase of the environmental problems regarding climate changes, scarcity of energy and greenhouse gases emissions, which increase the need of new environmentally beneficial technologies. Photocatalysis can also be used for water purification: many references are already present in literature on the degradation of dyes or drugs in aqueous solutions simulating the real pollution of rivers and lakes.

TiO_2 is very stable and very suitable for applications in environmental improvement and protection. Other than the antipollution properties, TiO_2, always in the anatase phase, is capable of conferring both self-cleaning and antibacterial properties to the surfaces [1].

Titanium dioxide is a semiconductor widely used in nanotechnology [2]. Since Fujishima and Honda discovered the phenomenon of photocatalytic water splitting [3], effort has been devoted to the research of TiO_2 materials, with potential applications in several fields, from biomaterials to self-cleaning processes and from sensing to photovoltaic applications, as well as in photocatalysis [4–6]. Indeed, it has been broadly studied for environmental applications, such as pollutant abatement both in liquid and in gas phase, and it has many advantages compared to other photocatalysts in particular because of low production cost and high chemical stability [7].

It is possible to find TiO_2 in three different crystallographic phases: anatase, rutile and brookite. Anatase is the most photocatalytically active; it has a bipyramid tetragonal symmetry, with four units per elementary cell (**Figure 1a**), and its structure consists in elongated octahedra. On the contrary, rutile is largely used as pigment and in the coating industry, precisely because of its chemical inertness; it is tetragonal, with two formula units per elementary cell (**Figure 1c**). Brookite is a metastable phase, and apart from a limited range of temperature and pressure, it easily turns in the other two forms; it has got an orthorhombic symmetry, with eight formula units per elementary cell (**Figure 1b**) [8].

Powdered TiO_2 is used as a common white pigment and effective opacifier thanks to its brightness and very high refractive index. More than 5 million tons of pigmentary TiO_2 are produced annually worldwide, and this amount is expected to increase as consumption continues to rise [9]. It is often used to provide whiteness and opacity in commercial products such as paints, coatings, plastics, papers, inks, foods, medicines (i.e. pills and tablets) as well as most toothpastes [10].

http://dx.doi.org/10.5772/62892

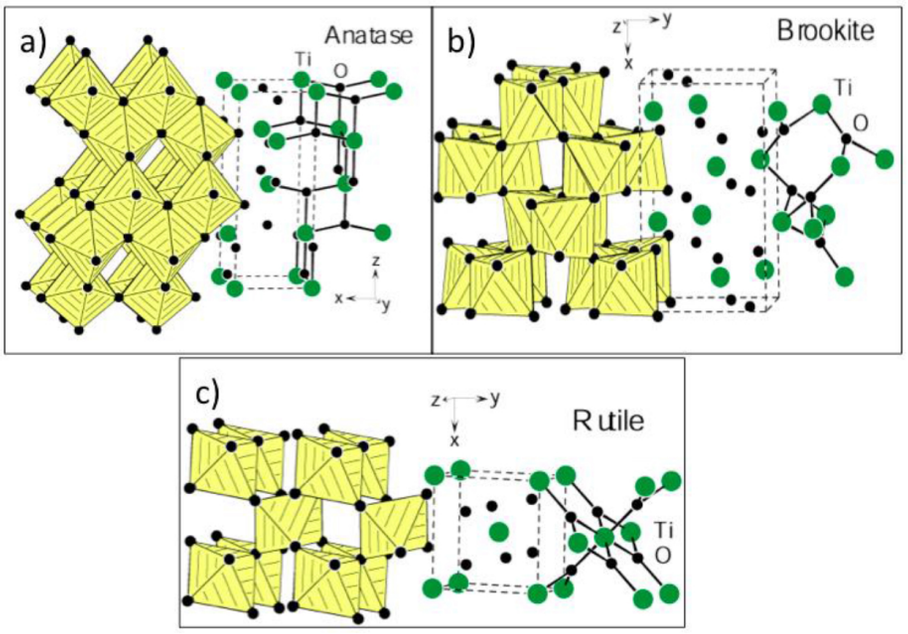

Figure 1. TiO_2 crystallographic phases: (a) anatase; (b) brookite; (c) rutile.

The use of nanomaterials (NMs) such as titanium dioxide in the production of cosmetics, sunscreens, surface coatings and some food products is widespread and successfully applied [11], as well as the most part of NMs has been used in products for health and fitness, including both medical/pharmaceutical and personal care products [12].

New physical and chemical properties emerge when the size of the material reaches the nanoscale. Firstly, the specific surface area increases dramatically as the size of a material decreases [13], and the high surface area brought about by small particle size is beneficial to many TiO_2-based devices, as it facilitates the interaction between the devices and the surrounding environment.

For this reason, in recent years nanotechnology has spread through all sectors of science and technology including engineering, medical, pharmaceutical, agriculture, environment and many more.

However, nanoparticles exhibit potential risks in terms of: (i) dispersibility, that is, the ability to disperse in the environment including potential long range transport; (ii) ecotoxicity, i.e. the ability to cause adverse effects to organisms in the environment; (iii) persistency, that is the ability to remain in the environment; (iv) bioaccumulation, that is the ability to either bioaccumulate or bioconcentrate in higher order organisms; (v) reversibility, i.e. the ability for removal or to reverse their original introduction from environment.

Human health risks associated with nanotechnology include both inhalation and/or exposure of/to nanoparticles or the ingestion of water or food and dermal contact [14]. The exposure to nanoparticles leads to a number of effects including oxidative stress, lipid peroxidation, genotoxicity, lung diseases, inflammation or pulmonary pathological changes [15–18].

In literature, there are many references that describe and present information on titanium dioxide health risks [19]. The International Agency for Research on Cancer (IARC) classified ultrafine TiO_2 as possible carcinogenic to humans [20]. The USA National Institute for Occupational Safety and Health reported that the exposure to ultrafine TiO_2 should be considered potentially carcinogenic [21] and the Federal Institute for Occupational Safety and Health showed some results of toxicokinetic analysis in lungs and in organs like liver and brain, finding a small solubility effect under physiological conditions, as well as lung tissue inflammation for exposures to high dose of TiO_2.

Moreover, TiO_2 inhalation studies prove to be injurious on rodents as well [15], as higher incidence of lung tumours was detected after exposure to ultrafine TiO_2 for 2 years in rats [22].

Thus, despite the good properties and the high efficiency of nano-sized TiO_2, these concerns over safety may limit its applications, and it is very important to find a replacement.

For this reason, the use of micrometric TiO_2 becomes more and more interesting and few years ago some investigations demonstrated the possibility to use this material for the photodegradation of pollutant molecules, such as volatile organic compounds (VOCs), nitrogen oxides (NO_x) or organic molecules that mainly pollute the water systems [23, 24]. It has also been successfully used in building materials to exploit self-cleaning and antibacterial effects [25].

Generally, micro-TiO_2 is usually used as a pigment but never in photocatalysis; however, as already mentioned, testing it for the photodegradation of different kinds of pollutants, both in gas and in aqueous phase, the efficiency of this material was confirmed at this point [1, 10, 24]. Furthermore, application of micro-TiO_2 in different materials, such as building materials and paintings, may bring many benefits, because when compared with nanometric TiO_2, it is easier to handle, cheaper as well, and shows a good photoefficiency [10].

The coating of TiO_2 allows conferring the material surfaces all the properties of TiO_2 as semiconductor [26]. It is already widely used on different materials, for different applications: on exterior construction materials [27, 28] for water [3] and air purification [29], for the preparation of self-cleaning and antibacterial cements [30], on tiles [23, 31], on glass [32], and, recently, for the protection of the cultural heritage [33]. Most of these materials are currently prepared with nanometric titanium dioxide, with all the ensuing problems described above.

Different techniques can be used to prepare and coat TiO_2 on solid supports, such as glass, metals or ceramics; to improve both adhesion and hydrophilicity of coating, silica can be added as a suspension, while several coating techniques, such as dipcoating, spincoating and spraycoating, can be used to spread the TiO_2 mixture over the support.

Among the several kinds of supports to obtain TiO_2-coated materials, with interesting photocatalytic properties that can be used in both outdoor and indoor environments, porcelain grés tiles are very attractive. When the industrial production began in the 1970s, porcelain grés tiles were aesthetically not very attractive and considered as just a technical material characterized by lack of porosity and strong resistance to both abrasion and acid attack. However, in the last decades, porcelain grés tiles underwent significant transformations in terms of appearance, mainly in size. Currently, thanks to advanced and innovative industri-

http://dx.doi.org/10.5772/62892

al production methods, both properties and appearances of these materials are improved and completely fit the market requests. In particular, the possibility to prepare slabs of large sizes (such as 300×150 cm) is the new frontier of building materials [23]. Porcelain grés tiles are manufactured under high pressure by dry-pressing fine processed ceramic raw materials with large proportions of quartz, feldspar and other fluxes and are characterized by a very low water absorption rate (less than 0.5%). In fact, these materials are fired at very high temperatures (1200–1300°C) in kilns [34]. A complete frost resistance due to the lack of porosity, complete waterproofing, durability, hardness and wear resistance properties thus characterizes the final ceramic product.

Besides these noteworthy architectural features, the deposition of anatase TiO_2 form converts the traditional ceramic into a photocatalytic eco-active material with the ability to reduce polluting molecules present in both air and water, to eliminate bacteria and to reduce the surface dirt thanks to the self-cleaning properties [35].

Self-cleaning refers to the pollutant degradation and dirt removal from surfaces, by their different behaviour towards water, relating to their hydrophobicity or hydrophilicity [36]. The main characteristic of superhydrophobic surfaces is high roughness, which implies low adhesion forces between contaminating particles and the surface, so water droplets roll off very quickly [37], and dirt can be very efficiently removed. On the contrary, TiO_2 confers the superhydrophilicity feature to the surfaces, under light irradiation, and water dropped onto titanium dioxide forms low contact angle. The Research Institute of Toto Ltd discovered the effect for a photocatalytic surface irradiated by sunlight in 1995.

There are two different ways to exploit the TiO_2 features for self-cleaning: (i) in the first case, TiO_2 nanoparticles are introduced inside a polymeric matrix in order to create nano-roughness on the surfaces and make them hydrophobic and superhydrophobic [38, 39]; (ii) secondly, the hydrophilicity of TiO_2 is the key property. Indeed, under UV exposure, titanium dioxide becomes super hydrophilic, and the decrease of the water contact angle creates a uniform water film on the treated surfaces, preventing contact between external dirt and surfaces themselves [40]. The main application is on building coverings because it decreases the periodicity of cleaning or renovation of the surfaces, maintaining their aspect as constant as possible [41].

The antibacterial properties are also important and interesting. They allow destroying the bacteria present at the photocatalytic material surfaces with the only action of light and humidity present in the air without using specific detergents, source of pollution for rivers and seas [42, 43]. Many bacteria have been investigated, and the photocatalytic antibacterial activity is always confirmed even with the most dangerous MRSA species, resistant to antibiotics [44].

In this chapter, we show two new frontiers in photocatalysis. Firstly, the real possibility to use a commercial micro-sized TiO_2 in powder form (K1077 by Kronos) as a photocatalyst is reported, with results compared with two traditional nanometric powdered samples (P25 by Evonik and PC105 by Cristal). Secondly, we report the industrial preparation of a photoactive porcelain grés tile, coated by spray method with the micro-sized TiO_2 (White Ground Active sample). In both cases, characterization results of both powders and tiles will be put in correlation with all the photocatalytic properties: antipollution in water (phenol) and air

(NO_x and VOCs), self-cleaning (oleic acid as reported in the standard ISO 27448 rule) and antibacterial investigating the degradation of *Escherichia coli* and *Staphylococcus aureus MRSA*.

The possibility to use micro-sized TiO_2 in a commercially manufactured product opens the way to a new generation of intrinsically safer materials than the traditional photocatalytic products for both workers in the factories and public safety.

2. Material and methods

Three commercial TiO_2 samples were selected without further treatment: two nano-sized by Evonik (P25) and by Cristal (PC105) and one micro-sized by Kronos (K1077).

Staring from the traditional porcelain grés tiles fired at 1200°C with a vitrified surface, photoactive porcelain grés tiles by GranitiFiandre S.p.A were prepared covering the surface with an aqueous mixture of pure anatase micro-TiO_2 in powder form (K1077) and a commercial SiO_2-based compound by spray method in airless cabins. To ensure the semiconductor strong adherence and the complete surface vitrification, given by the presence of SiO_2, tiles were heated at 680°C for 80 min in an industrial kiln and then brushed to remove TiO_2 particles present at the ceramic surface and not completely stuck (sample name: White Ground Active, i.e. WGA) [21; Patent n. EP2443076].

2.1. Sample characterization

We used the following equipments to characterize the powdered samples. N_2 adsorption/desorption measurements at 77 K Brunauer–Emmett–Teller method (BET) using Sorptometer instrument (Costech Mod. 1042) to investigate specific surface area (SSA) of all samples.

X-ray diffraction (XRD) with a PW3830/3020 X'Pert diffractometer from PANalytical working in Bragg-Brentano geometry (Cu Kα1 radiation; k = 1.5406 Å) was chosen to inspect the crystalline nature of the samples.

High-resolution transmission electron microscopy (HR-TEM) using a JEOL 3010-UHR instrument (acceleration potential: 300 kV; LaB6 filament) was used to detect the fine morphology of the materials (powder form). Samples were always 'dry' dispersed on lacey carbon Cu grids.

X-ray photoelectron spectra (XPS) were obtained in an M-probe apparatus (surface science instruments) using a monochromatic source of Al Kα radiation (1486.6 eV).

For the band-gap determinations, diffuse reflectance spectra of the materials in powder form were recorded employing a UV-Vis scanning spectrophotometer (PerkinElmer, Lambda 35 model), equipped with a diffuse reflectance accessory. The Kubelka-Munk function was used to elaborate data to determine the band gap values by performing the first derivative of the Kubelka-Munk equation.

In situ FTIR spectroscopy was used to detect the surface functionalities, mainly surface hydroxyl species. Absorption/transmission IR spectra were collected at room temperature (RT)

http://dx.doi.org/10.5772/62892

on the samples outgassed in vacuo at RT by means of a Perkin-Elmer FT-IR System 2000 spectrophotometer equipped with a Hg-Cd-Te cryo-detector. Spectra were collected in the 7200– 580 cm^{-1} range at 2 cm^{-1} resolution. For this analysis, the powdered photocatalyst was pressed in self-supporting pellet (~10 mg cm^{-2}), placed in a homemade quartz cell, equipped with KBr windows, connected to a conventional vacuum line.

High-resolution SEM-EDX investigations were performed on ceramic tiles using a field emission gun electron scanning microscopy LEO 1525, while the elemental composition was obtained using Bruker Quantax EDS.

2.2. Photocatalytic tests

2.2.1. VOCs (volatile organic compounds)

The photodegradation of some VOCs (i.e. acetone, acetaldehyde, ethanol and toluene) was monitored conducting the degradation in a Pyrex glass cylindrical reactor with diameter of 200 mm and effective volume of 5 L [25]. For each test, 0.05 g of photocatalyst (in powder form deposited on flat glass disk from a 2-propanol slurry) was used. Hot chromatographic air, humidified at 40%, and a fixed amount of the volatilized VOC were mixed to obtain the requested gaseous mixture in the reactor. The actual concentration of the organic molecule in the reactor was determined directly by micro-GC sampling as shown in **Figure 2**. Photon sources were provided by a 500 W iron halogenide lamp (Jelosil, model HG 500) emitting in the 315–400 nm wavelength range (UV-A) at 30 Wm^{-2}. The duration of each test was selected by considering the difficulty in degrading a molecule, in a time between 2 and 6 hours. The intermediate oxidation products were determined directly by investigating the sample surface after the kinetic run by FTIR spectroscopy and the determination of CO_2 was performed by gas chromatography as well.

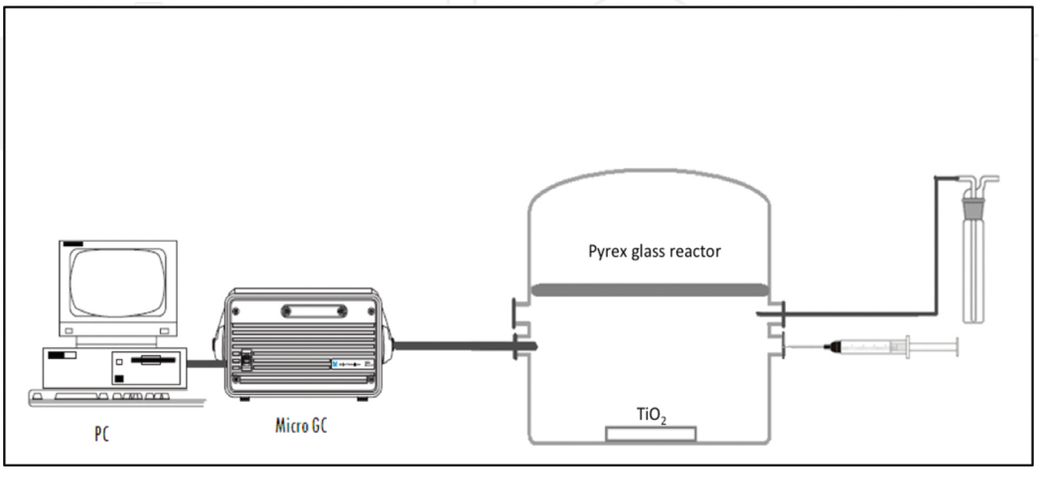

Figure 2. VOC photodegradation—set-up.

2.2.2. NO_x

• *Static condition*

The photocatalytic activity of both powder samples was tested in NO_x degradation, operating in static conditions in a Pyrex glass cylindrical reactor with an effective volume of 25 L [10]. The amount of catalyst used in the tests in this case was 0.05 g.

NO_2 (0.6% in nitrogen) was mixed with air humidified at 40% to obtain the gaseous mixture in the reactor. It is important to underline that we start from an inlet gas of pure NO_2 pulsed into the reactor that, as soon as it comes into contact with the air present inside the vessel, reaches the chemical equilibrium between NO and NO_2 so as to naturally obtain the NO and NO_2 mixture in air. Different concentrations of NO_x in the reactor were chosen: i) 1000 ppb in order to follow the same pollutant concentration requested by the ISO 22197-1 rule; ii) 200 ppb that is very close to the alert threshold set by the EU Directive 2008/50/CE for NO_2. Photon sources were provided by a 500 W iron halogenide lamp (Jelosil, model HG 500) emitting in the 320–400 nm wavelength range (UV-A), but with a specific UV power on the surface of the samples set at 10 Wm^{-2}. The NO_x photocatalytic tests were performed at 30°C and lasted for 4 or 6 hours. The actual concentration of pollutants (NO, NO_2 and consequently their sum, i.e. NO_x) in the reactor was determined in this case directly by a chemiluminescence (Teledyne, Mod. 200E).

• *Continuous flow reactor*

The photoefficiency towards the NO_x degradation of tiles of 600×600 mm was confirmed using a purpose-built reactor [45]. The continuous flow reactor (**Figure 3**) has walls of 10 mm of thickness and an internal size of 625×625×115 mm with four inlets and one opposite outlet and can house a sample of 600×600×10 mm. This configuration assures a good homogeneity of the reactants in the gas phase and a contact between reactant and photocatalytic tiles that well reproduces the real working conditions.

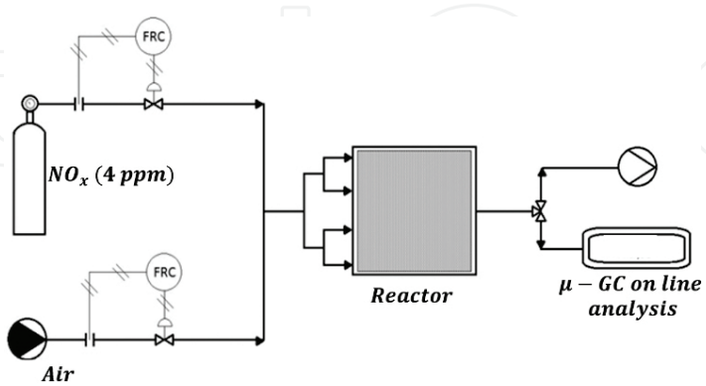

Figure 3. Scheme of the experimental continuous NO_x set-up.

Reactor is equipped with a thermo-hygrometer model HT-3006A to measure both temperature and humidity during the tests. Humidity inside the reactor is maintained constant

http://dx.doi.org/10.5772/62892

between 40–50% through bubbling the gas flow into a gas bubbler (containing water and saturated aqueous vapour). The irradiation was emitted by two iron halogenide lamps (Jelosil, model HG 500) positioned at 770 mm centre-to-centre distance. The light intensity incident on the sample surface in the UV-A region was measured with a Delta Ohm radiometer and regulated at 20 Wm^{-2} by adjusting the distance of the lamp from the reactor. The degradation was performed at different initial NO_x concentrations, obtained by diluting the stream of NO_x from the cylinder with air, at RT and working with a total gas flow of 140 and 180 NL h^{-1}. The concentration values were chosen to work closely to the limit values reported on the Directive 2008/50/EC, in particular, 106 ppb (equal to 200 μg m^{-3}, value not to be exceeded more than 18 times in a calendar year) and 213 ppb (400 μg m^{-3}, alert threshold).

2.2.3. Liquid phase

Regarding photocatalytic tests in liquid phase, the experimental set-ups are different depending on whether we use powders or tiles.

• *Photocatalytic test using powdered nano- and micro-TiO_2 catalysts*

Dye degradation in water media was performed in a slurry reactor, equipped by an internal refrigerating serpentine system (**Figure 4a**) of 0.5 L volume [44]. Irradiation was allowed by the use of an external UV-A lamp (500W, Jelosil®, HG500, halide lamp), emitting in the range 315–400 nm and with a power evaluated by a radiometer instrument (Delta OHM, model HD2102.2) of 75 Wm^{-2}. A UV-Vis spectrophotometer analyzer (T60 UV-Vis PG LTD instrument) has been used to measure the concentration of dyes or organic molecules as a function of time.

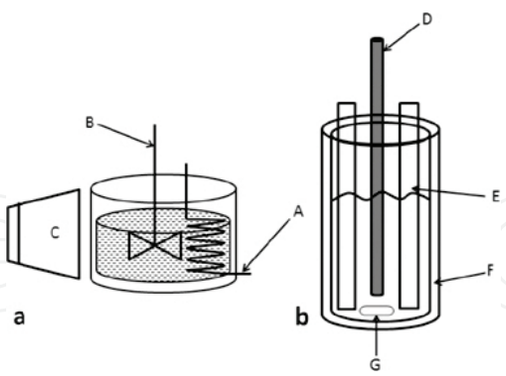

Figure 4. Liquid phase reactors: a) Continuous stirred slurry reactor. A: refrigerating serpentine system; B: Stirrer; C: UV lamp. B) Cylindrical batch reactor used for photocatalytic experiments. D: UV lamp; E: photocatalytic tiles; F: cooling jacket; G: magnetic stirrer.

• *Photocatalytic test using photoactive TiO_2 tiles*

A cylindrical batch reactor of 1 L volume, refrigerated with a cooling jacket, was used for dye degradation tests in the presence of 10 photoactive tiles (0.03 m^2 total surface photoactive area)

immersed into the liquid solution, as schematically shown in **Figure 4b** [46]. In this case, two different lamps directly immersed into the aqueous solution were used: a typical germicidal W UV lamp (Philips TUV BL-S, model AEPL-7913 mercury vapour low pressure), with an UV-A illuminance at the tile surface of 1 Wm^{-2} and a 125 W UV-A lamp (Jelosil, mercury vapour low pressure), with an illuminance of 65 Wm^{-2}.

2.2.4. Self-cleaning

The ISO 27448 rule was precisely followed to perform the measurements on tiles. The *self-cleaning* action is assessed by measuring the contact angle generated by the film of pure oleic acid and by monitoring the changes in the angle due to any degradation of the deposited acid due to the UV irradiation. Only if the surface has photocatalytic properties, the changes of the contact angle value occur.

The contact angle was measured (Kruss instrument equipped with high resolution TV camera) after the cleaning pre-treatment by UV irradiation, after contact with the oleic acid (zero time) and after irradiation with UV lamp at 20 Wm^{-2} at 2, 4, 6, 24, 48, 72, 74 and 76 hours. At each time, the measurement is repeated on five random points on the surface of the tested material.

Samples of WGA (size 100×100 mm), randomly taken from an industrial production batch, were placed in a suitably prepared solution containing 0.5 vol% of oleic acid (Fluka reagent, purity >80%) in n-eptane (Fluka reagent, purity >99%), in order to obtain a uniform coating of oleic acid at the surface. The amount of oleic acid thus applied resulted to be 2.0 ± 0.2 mg, (value measured by means of a Gibertini Elettronica precision balance). An additional sample of WGA was pre-treated and then coated with the oleic acid using the same method. At the end of this procedure, the additional sample was then placed in a vessel in the dark with controlled air and humidity, throughout the duration of the whole test (76 hours).

2.2.5. Antibacterial efficiency

The measure was performed on photocatalytic tiles following the ISO 27447:2009 rule (film adhesion method) (rif. ISO 27447:2009 Fine Ceramics (Advanced Ceramics, Advanced Technical Ceramics)—Test Method for Antibacterial Activity of Semiconducting Photocatalytic Materials, 2009).

The test used *E. coli* ATCC 8739 and *S. aureus* ATCC 43300 methicillin-resistant MRSA. Each strain was inoculated into a nutrient agar slant, incubated for 16–24 hours at 37°C ± 1°C and subsequently transferred in a new nutrient agar slant and again incubated at 37°C ± 1°C for 16–20 hours. An adequate quantity of bacteria was dispersed in 1/500 NB (nutrient broth) to obtain a count of 6.7×10^5 to 2.6×10^6 cells/ml. Samples of 50×50 mm square was rinsed with distilled water and autoclaved at 121°C for 30 minutes before the test to remove any organic residue present at the ceramic surface. For each bacterium strain were tested specimens without antibacterial treatment and six specimens with antibacterial treatment; 0.15 ml of bacterium suspension was put onto each specimen and covered with a 40×40 mm square inert and non-water adsorbent film with a transparency rate over 85% for the 340–380 nm range. Each specimen was placed in a 100 mm diameter Petri dish containing moistened paper filter

http://dx.doi.org/10.5772/62892

to prevent drying out of the suspension covered with a 1 mm thickness borosilicate glass with a transparency rate over 85% for the 340–380 nm range.

The samples were irradiated with a fluorescent UV lamp (18W Philips PL-L) with an intensity of 0.25 $mWcm^{-2}$ for 8 hours. A similar sample was treated with the same procedure but left in the dark for the whole test. A viability count was performed by dilution and plating on nutrient agar (NA) incubated at 37°C for 48 hours [45].

The bacterium concentration of the washout liquid is obtained by Eq. 1 and expressed to two significant digits:

$$P = Z \times R \tag{1}$$

where *P* is the bacteria concentration (cells/ml); *Z* is the average number of colonies in two Petri dishes; *R* is the dilution factor. When the number of viable bacteria is less than 30 in the Petri dishes with 1 ml of washout solution, the cell number is used to calculate the average number.

The bacteria concentration obtained in Eq. (1) is applied in Eq. (2) to calculate the number of viable bacteria.

$$N = P \times V \tag{2}$$

where *N* is the number of cells of viable bacteria; *P* is the bacteria concentration obtained in Eq. (1) (cells/ml); *V* is the volume of Soybean-casein digest broth with lecithin and polysorbate (SCDLP) medium for washout (ml).

Equations (3) and (4) are necessary to calculate the photocatalyst antibacterial activity value after the test is completed.

$$R_L = \left(\log\left(B_L/A\right) - \log\left(C_L/A\right)\right) = \log\left(B_L/C_L\right) \tag{3}$$

where R_L is the photocatalyst antibacterial activity value, after UV irradiation of intensity *L; L* is the UV irradiation intensity ($mWcm^{-2}$); *A* is the average number of viable bacteria of non-treated specimens, just after inoculation; B_L is the average number of viable bacteria of non-treated specimens, after UV irradiation of intensity *L;* C_L is the average number of viable bacteria of photocatalytic treated specimens, after UV irradiation of intensity *L*.

$$\begin{aligned} \Delta R &= \log\left(B_L/C_L\right) - \left(\log\left(B_D/A\right) - \log\left(C_D/A\right)\right) \\ &= \log\left(B_L/C_L\right) - \log\left(B_D/C_D\right) \end{aligned} \tag{4}$$

where ΔR is the photocatalyst antibacterial activity value with UV irradiation; B_D is the average number of viable bacteria of non-treated specimens, after being kept in a dark place; C_D is the average number of viable bacteria of photocatalytic treated specimens, after being kept in a dark place.

3. Results and discussion

3.1. Characterization

3.1.1. Commercial powders of TiO_2

The XRD patterns relative to the three selected samples are reported in **Figure 5**. Anatase is the unique polymorph present for all samples, except for the well-known P25 material, which exhibits the 80:20 anatase/rutile ratio phase composition. The crystallographic reflexes (1 0 1), (2 0 0) and (2 1 1) have been used to calculate the average crystallite size of the various titania particles (**Table 1**, third column). P25 and P105 possess comparable crystallite size centred at around 25 nm, while the sample K1077 exhibit a value of 130 nm. These features are reflected in the BET surface area of the micro-sized sample (K1077), which is much lower compared to the nano-sized ones (**Table 1**, second column).

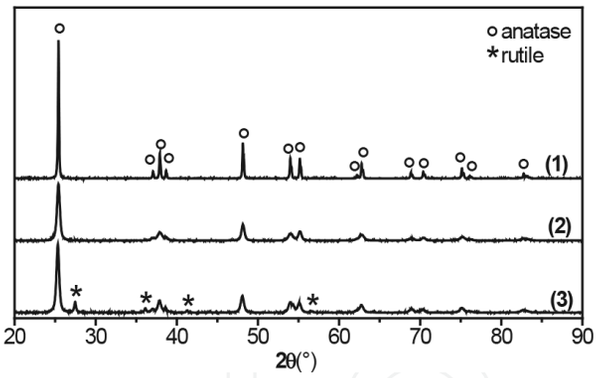

Figure 5. XRD patterns of K1077 (1), PC105 (2) and P25 (3).

Sample	BET surface area (m^2g^{-1})	Average crystallite size (nm)	XPS Ti $2p_{3/2}$ (eV)	XPS OH/O_{tot}	Band gap (eV)
P25	50	26	458.4 ± 0.1	0.14	3.21
PC105	80	23	458.4 ± 0.2	0.85	3.19
K1077	12	130	458.3 ± 0.1	0.32	3.15

Table 1. Main features of commercial TiO_2 samples.

A comparison between the morphological features exhibited by the nano-sized powders, respectively known as P25 and PC105, and the micro-sized K1077, was carried out by TEM.

http://dx.doi.org/10.5772/62892

TEM images (**Figure 6**) confirm the above average crystallite size extrapolated by XRD analysis also excluding the presence of ultra-fine particles in K1077. It can also be evidenced that the nano-sized materials perfectly fall within the 'nano' definition: in fact, both nano-samples are characterized by average particles size of 15–30 nm; they exhibit a closely packed nature and almost roundish contours. However, the highly crystalline nature of these powders is confirmed by the high incidence of fringe patterns, which are generated by the superimposition of crystals almost all belonging to the TiO_2 anatase polymorph. In both cases, the prevalently observed planes (d = 0.357 nm) are ascribable to the (1 0 1) family (ICDD anatase file no. 21-1272).

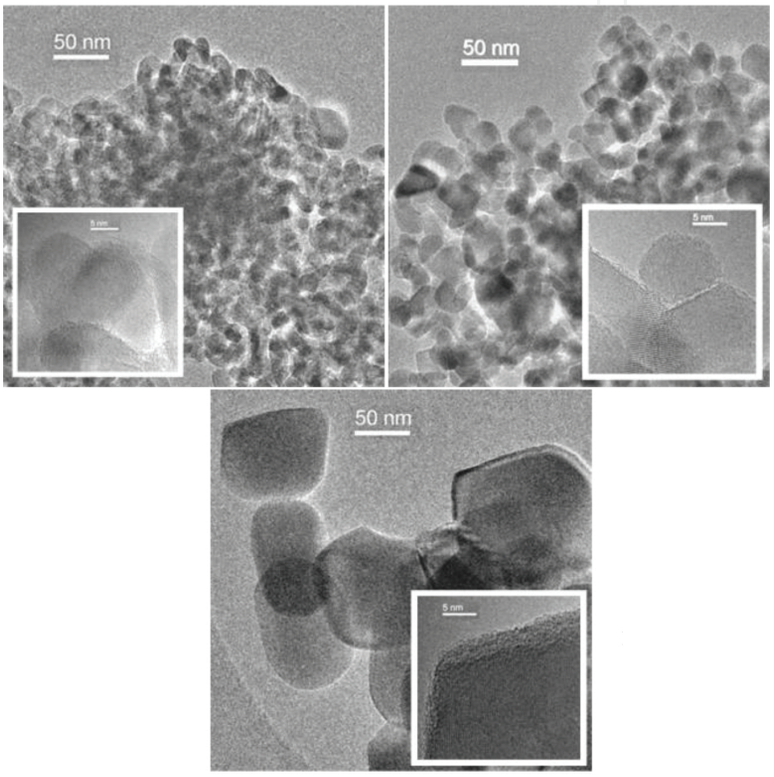

Figure 6. Top left-hand image refers to PC105, top right-hand image refers to P25 and bottom image refers to K1077.

As far as the micro-sized sample is concerned, much larger average dimensions of the particles (**Figure 6**) are observed. This feature is in total agreement with the indications obtained by means of XRD analysis, evidencing the average dimensions in the 120–200-nm range for the K1077 sample. Moreover, also in this case the most frequently observed crystal planes are those belonging to the (1 0 1) family of the TiO_2 anatase polymorph, thus exhibiting a much less defective nature of the particles.

XPS was used to detect the surface state of the TiO_2 particles by (**Figure 7**). No significant differences can be appreciated among all the investigated samples in the Ti 2p region concerning both binding energies (BE) and full width at half-maximum (FWHM) values. The Ti $2p_{3/2}$ peak is always present as a single doublet and the BE (forth column in Table 1) compares

well with the data for Ti(IV) in TiO_2 [48]. The analysis of the oxygen peaks exhibits the presence of two different components, which can be attributed to lattice oxygen in TiO_2 (529.9 eV) and to surface OH species (>531.5 eV), respectively [49]. For PC105, a particular O1s shape was observed (**Figure 7b**): in fact, the OH component is very intense probably due to a particular industrial synthesis in order to enhance the photocatalytic efficiency of the sample.

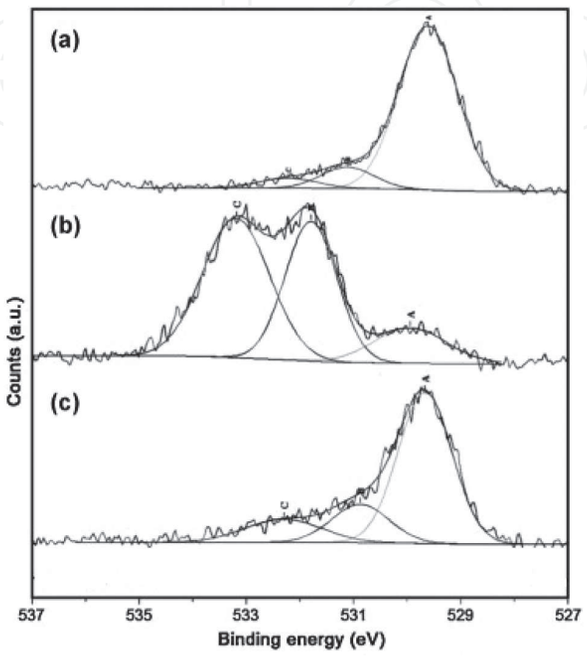

Figure 7. O1s XPS spectra for (a) P25; (b) PC105; (c) K1077.

The hydrophilicity/hydrophobicity character of photocatalyst surface plays a crucial role in determining the adsorption step and thus the photocatalytic activity in the degradation of pollutants [50]. The OH/O_{tot} surface ratio, reported in the fifth column of **Table 1**, is a quantitative measure of the hydrophilicity/hydrophobicity of the TiO_2 surface, estimated using the XPS-determined surface OH atomic concentrations normalized by the total oxygen atomic concentrations (O_{tot}) [51]. PC105 exhibits the highest concentration of OH that represents the 85% of the oxygen at the surface as previously underlined. It is noteworthy that the micro-sized sample presents a higher atomic concentration of OH groups in comparison with P25, pointing out the higher hydrophilic character of its surface.

From XPS spectra, we can obtain both the information on the BE of a specific element and the total density of states (DOS) of the valence band (VB) [52]. This measurement is useful to unravel the effect of TiO_2 structural modifications on the electronic properties of the material. Comparing semiconductor nanoparticles/microparticles, the quantum size effect could also play a role, giving band-gap narrowing in the bigger-sized particles in respect to the smaller ones. **Figure 8** reports the VB XPS spectra of both nano-sized samples and the micro-sized one. The VB maximum position was determined through linear extrapolation and the same values around −2.6 eV were measured for all samples, which is a typical value for TiO_2 [53].

http://dx.doi.org/10.5772/62892

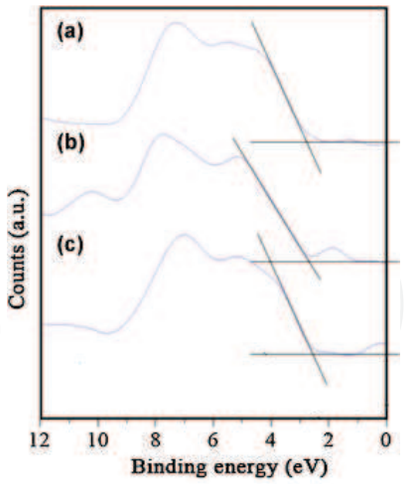

Figure 8. VB XPS spectra along with VB maximum determining by the linear extrapolation method for (a) P25; (b) PC105; (c) K1077.

Experimental data of diffuse reflectance were elaborated to absorption coefficient values F(R) according to the Kubelka-Munk equation (Eq. 5),

$$\frac{f(R_\infty) = (1 - R_\infty)^2}{2R_\infty} \tag{5}$$

where *R* is the reflectance.

The corresponding band gap values obtained by this procedure for all samples are reported in **Table 1** (sixth column). The obtained band gap values do not exhibit large differences among the various samples and fall in the range expected for the TiO_2 material.

3.1.2. Photocatalytic active tiles

Basic features of the porcelain grés tiles were determined after the coverage with the photocatalytic mixture to verify that the coating procedure does not alter the ceramic body. Lack of porosity, resistance to surface abrasion and durability were measured by water absorption [54], rotation of an abrasive load on the tile surface [55] and determination of frost resistance [56], respectively. The frost resistance determination is an intrinsic measurement of the product durability.

The coating with the SiO_2-based compounds and the following calcination step preserve the pure anatase form verified by XRD measurements [35]. The presence of SiO_2, together with TiO_2, enhances the formation of hydroxyl radical •OH, which would be achieved via strong Brønsted acid sites at the TiO_2/SiO_2 interface region [57]. This incorporation inhibits the crystal growth of TiO_2 allowing the preservation of the anatase structure at 680°C [58].

SEM images of WGA show a homogeneous distribution of the micro-sized TiO_2 crystallites without ultrafine particles (**Figure 9**), on the porcelain tile surface. If measurement is carried

out at higher magnification (**Figure 9**, at the bottom), it is possible to observe that the particle dimension falls in the 100–125 nm range, while at lower magnification it is possible to evidence larger particles of SiO_2.

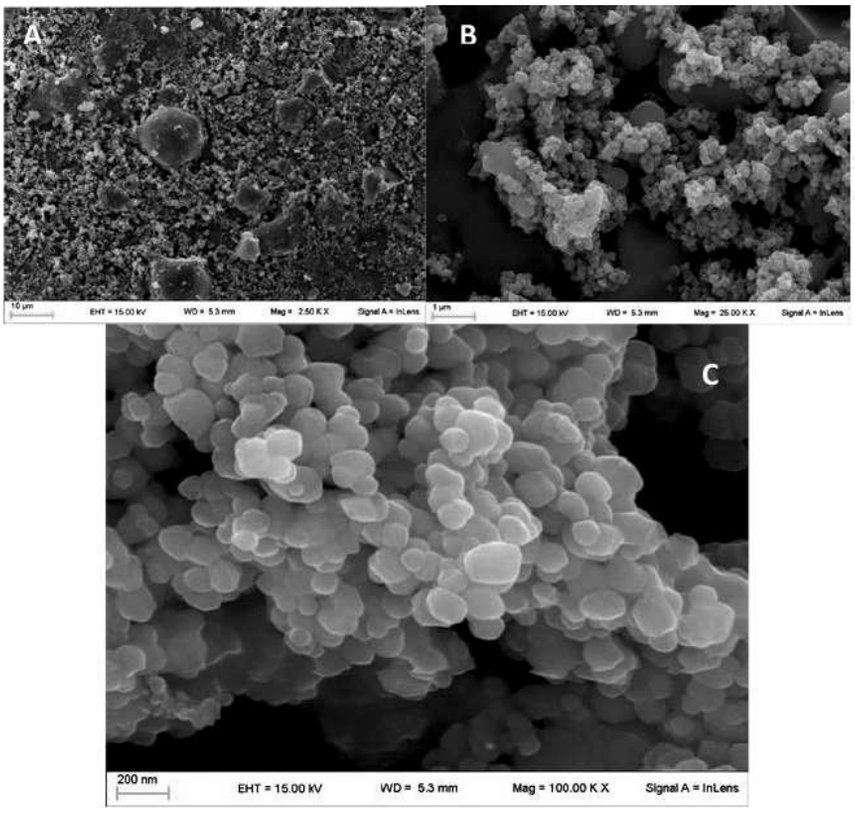

Figure 9. SEM images of photocatalytic active tiles (WGA at different magnifications: (a) 2.50 K X; (b) 25.00 K X; (c) 100.00 K X).

Wettability measurements were performed on both a grés tile and a photocatalytic active tile (**Figure 10**), exhibiting a completely different surface; in fact, the photocatalytic WGA tile presents very hydrophilic surface features with an average angle of 23.0°, which can be explained by the super hydrophilic property of TiO_2 photocatalyst [59].

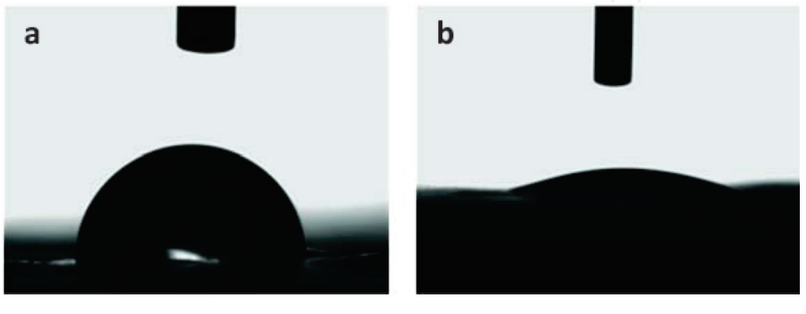

Figure 10. Contact angle: (a) traditional porcelain grés tile; (b) photocatalytic WGA tile.

http://dx.doi.org/10.5772/62892

3.2. Photocatalytic tests

3.2.1. Nano- and Micro-TiO_2 commercial samples

The results obtained with the commercial catalysts starting from 1000 ppb of NO_x are reported in **Figure 11**, and it is well evident that all samples show good photocatalytic performances. In particular, after 60 minutes of reaction, the NO_x conversion is almost complete. From this point, the actual difference between the nano-powder and the micro-one is evident, because while P25 reaches a complete degradation of NO_x, K1077 is not able to degrade the entire NO_x amount, even if it is able to convert more than 90% of the pollutant approximately. Thus, even if the nano-sized material exhibits the best performances, the photocatalytic activity of the pigmentary sample is very good, in agreement with the presence of appreciable amount of surface hydroxyls.

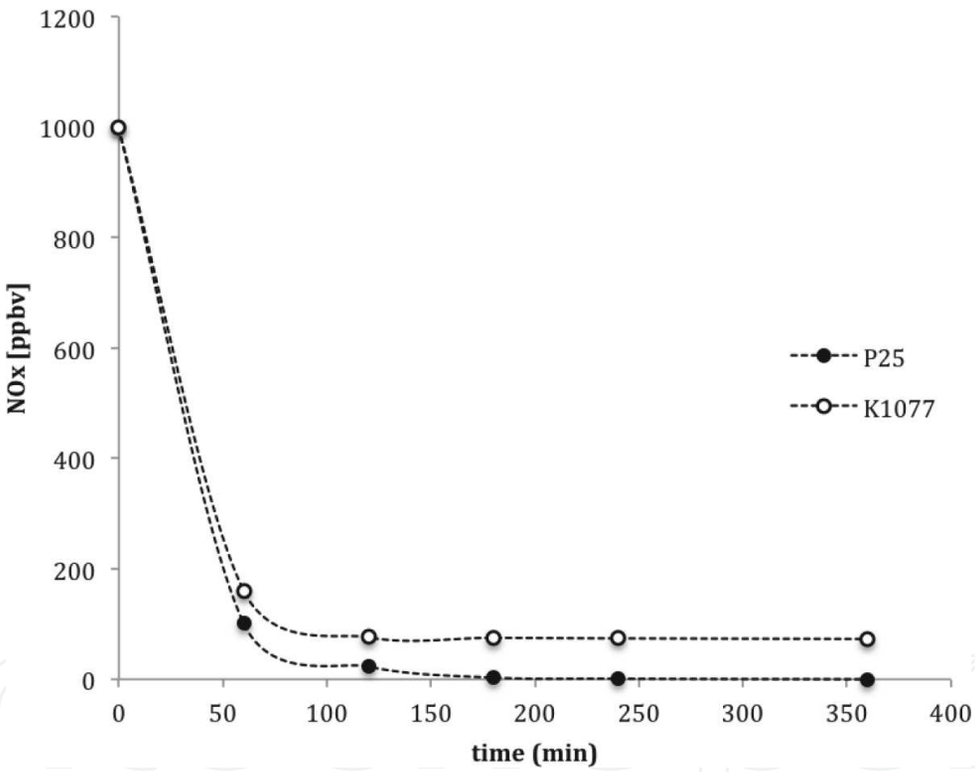

Figure 11. Comparison between nano-TiO_2 (P25; full dots) and micro-TiO_2 (K1077; empty dots).

Moreover, the results obtained using lower NO_x concentration show that nano-sized and micro-sized powders have a similar photocatalytic activity. Both samples reach the complete NO_x degradation within 50 minutes. Testing the materials in more diluted initial concentrations, the difference between micro and nano-samples is highly limited, and this means that the amount of surface OH species on the K1077 is enough to guarantee performances similar to that of P25, as also evident in **Figure 12**, relative to the FTIR features typical of OH species present at the surface of the three TiO_2 systems, after evacuation at RT.

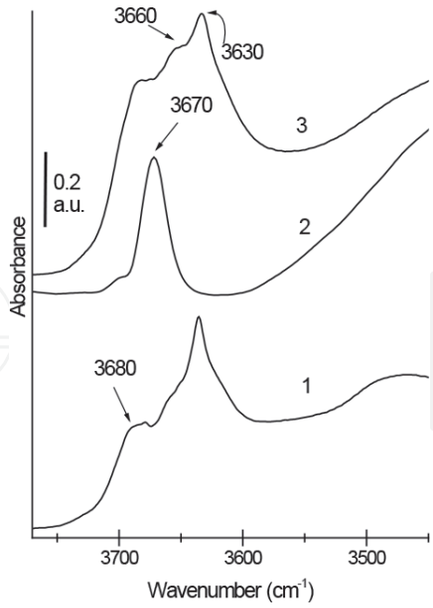

Figure 12. IR. Absorbance IR spectra relative to the OH stretching spectral region of samples outgassed at RT for 60 min: (a) P25; (b) K1077; (c) PC105.

Nano- and micro-sized commercial sample photoactivity has been studied also for the degradation of different VOCs (acetone, acetaldehyde, toluene and ethanol), as shown in **Figure 13** for the K1077 sample. VOC molecules are very interesting to study because they are mainly responsible for both outdoor and, even more, indoor pollution [60, 61].

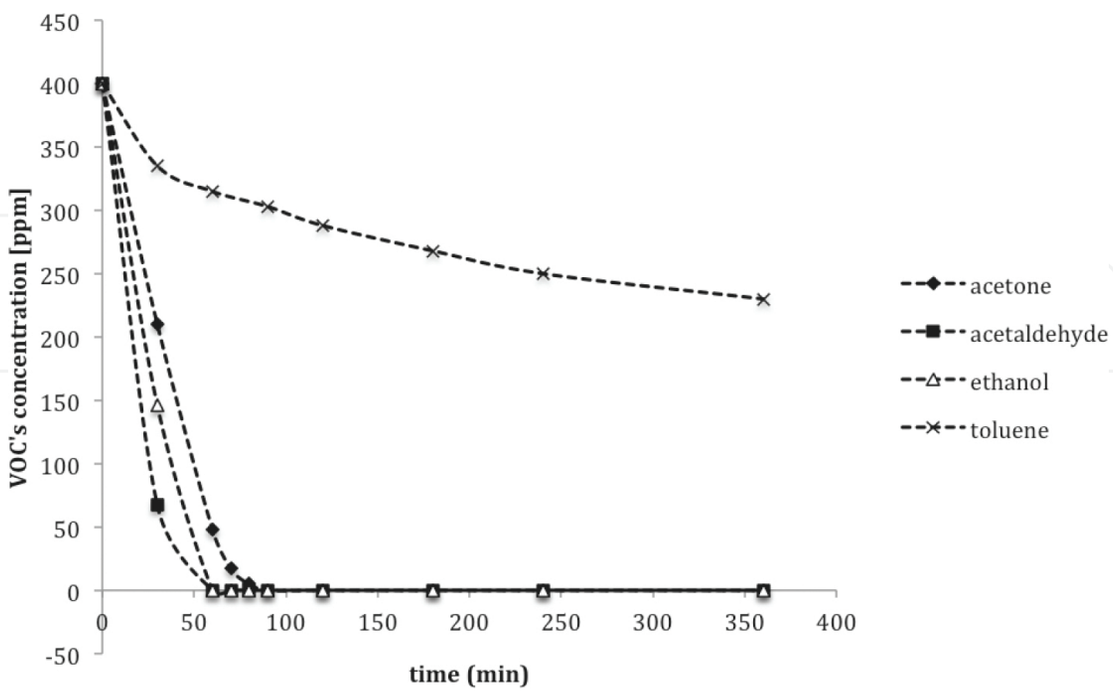

Figure 13. K1077 in the photodegradation of some VOCs.

http://dx.doi.org/10.5772/62892

Acetone reaction pathway passes through the formation of acetaldehyde as a by-product (**Figure 14a**) as reported by Stengl et al., while toluene is a less polar and less hydrophilic VOC, with a degradation that is more difficult because of the presence of the aromatic ring. Moreover, the degradation pathway of toluene passes through many by-products, which are not so easy to degrade and that in most cases are adsorbed on the TiO_2 surface (**Figure 14b**).

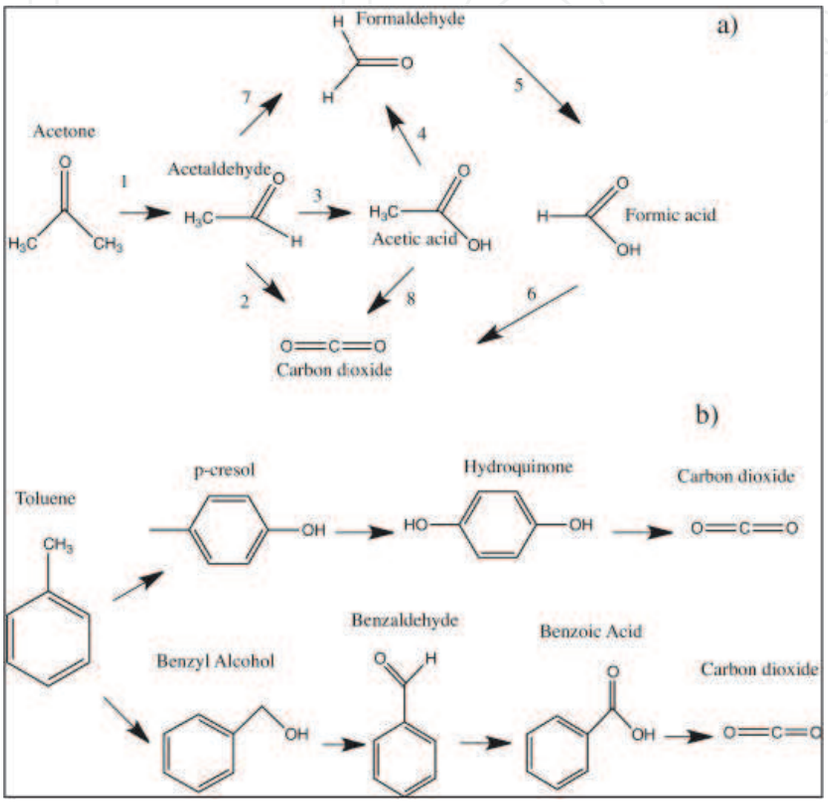

Figure 14. Reaction pathways of photocatalytic: (a) acetone oxidation; (b) toluene oxidation.

The nano-sized samples exhibit higher photocatalytic efficiency, leading to the complete pollutant degradation within a shorter reaction time, than the micro-sized K1077 sample. For acetone, acetaldehyde and ethanol, using both nano- and micro-sized powders, CO_2 is the only final product of the reaction, confirming the complete degradation without the formation of by-products adsorbed on the sample surface (verified by FTIR measurements on the sample surface after the kinetic runs). The case of toluene is different: for all samples, the pristine pollutant is not completely degraded even after 6 hours of reaction, and most of the by-products are not completely degraded, as well.

Considering surface area and particle size, the VOC photodegradation kinetic is faster when the particle crystallite size is smaller. The nature of the reactive sites is influenced by the morphological features of crystallites, thus inducing different type of exposed OH reactive sites onto the surface of nano- and micro-sized TiO_2 samples. Despite the low surface area, K1077 presents an abundant OH radicals' population, thus it shows to be able to photo-degrade

several VOCs, with not excessive differences in terms of performance compared to nano-TiO_2 powders.

3.2.2. Photocatalytic active tiles

Micrometric titanium dioxide can be used with very good results for the photocatalytic abatement of pollutants, such as NO_x or VOCs. Thus it has been industrially applied on porcelain grés tiles with many advantages in terms of (i) ease of manipulating micrometre powders instead of nano-powders, (ii) cost, because pigmentary TiO_2 is cheaper and (iii) safety, because of the toxicity of TiO_2 nanoparticles that can be inhaled.

The photocatalytic active tiles, obtained after the TiO_2 coating as described above, have been tested in the photodegradation of both gas and liquid pollutants, in particular studying their photocatalytic performances for the photodegradation of NO_x in gas phase, and for the photodegradation of phenol in liquid phase. Particularly, nitrogen oxides are the worldwide air pollution reference.

When tested for the NO_x abatement, photocatalytic active tiles show very good results. The pollutants are successfully degraded and the maximum conversion is reached just after about 40 minutes. The experiments of this run were performed at 140 NL h^{-1} and with a starting concentration of 100 ppb of NO_x (**Figure 16**). These experiments were conducted changing the parameters, in particular the NO_x starting concentration, as well as the duration of the reaction, obtaining in all cases good results [10].

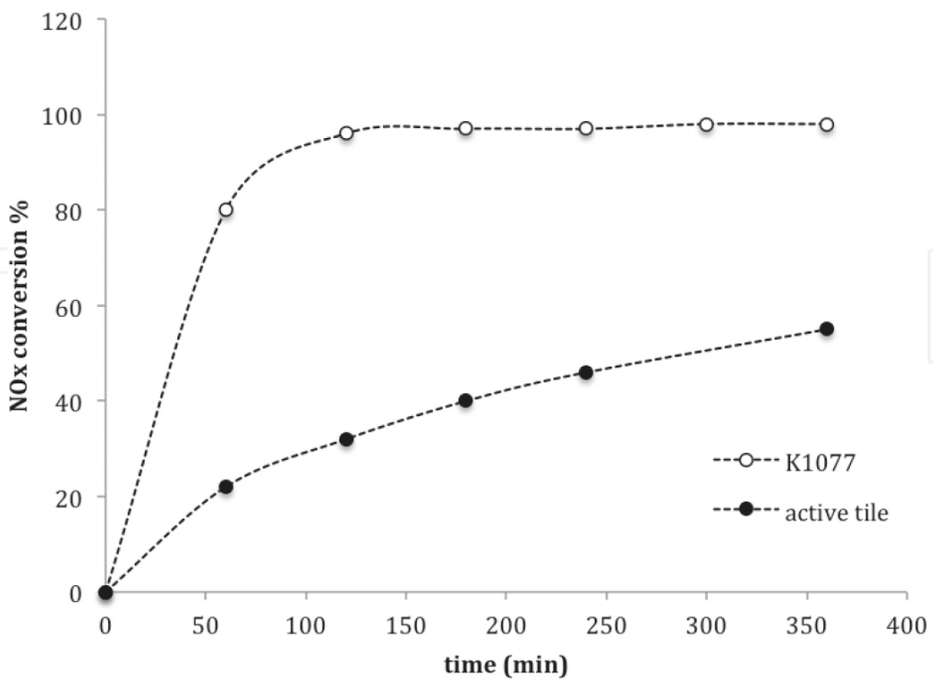

Figure 15. NO_x conversion % vs. time; comparison between K1077 (empty dots) and WGA (full dots).

http://dx.doi.org/10.5772/62892

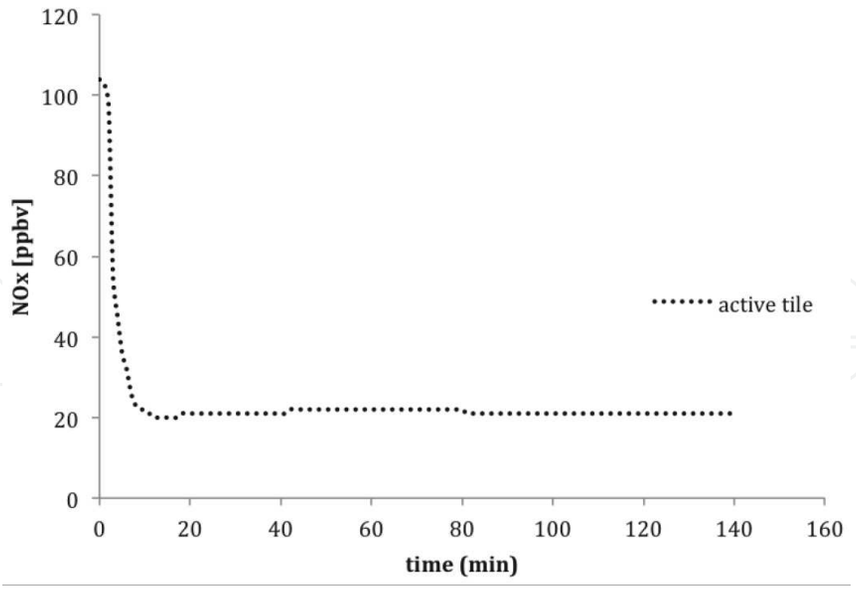

Figure 16. NO_x photodegradation using a WGA tile (3600 cm^2)—continuous flow reactor.

Investigating the phenol removal in water in the presence of WGA, it was observed that the trend of the degradation processes depends on the pollutant starting concentration. After 6 hours of exposure, the phenol photodegradation percentage is almost the same at 15 and 25 ppm (78 and 73%, respectively), and much lower at 50 ppm (46%), as shown in **Figure 17**.

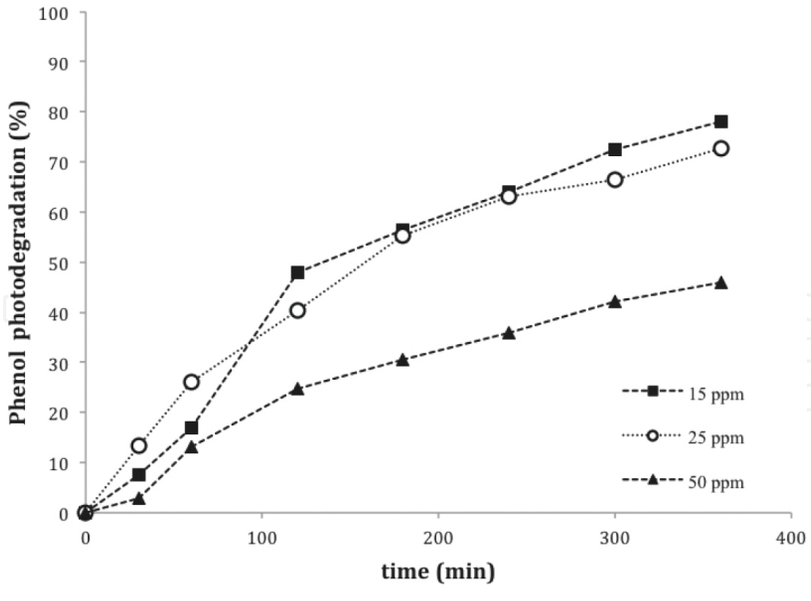

Figure 17. Photocatalytic degradation of phenol in the presence of WGA at different starting concentrations (15, 25 and 50 ppm, respectively)—influence of the starting phenol concentration on the reaction rate.

The mineralization data show that at the lowest concentrations, the pollutant adsorption is followed immediately by its degradation and mineralization; on the contrary, at higher

concentrations, the mineralization process starts later, and it is related to the hydroquinone formation, that is the main by-product (see **Figure 18**).

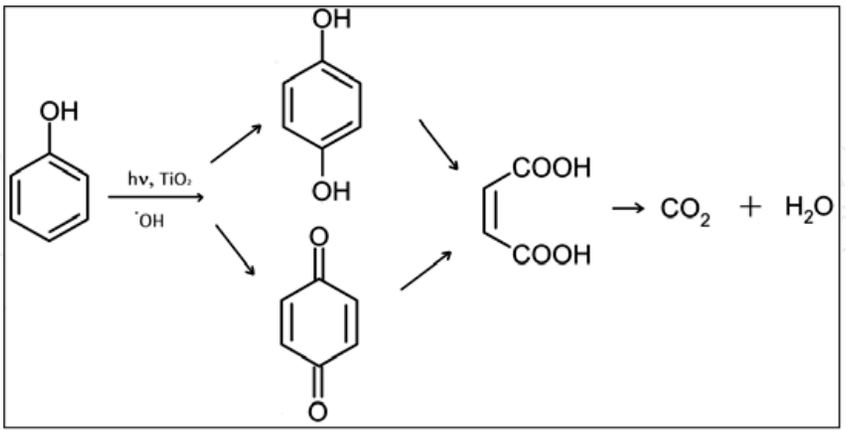

Figure 18. Degradation pathway of phenol photodegradation.

Therefore, the photocatalytic tile performances strongly depend on the starting pollutant concentration; anyway, photocatalytic tiles are able to degrade also the organic molecule, and they are effective in liquid phase.

These tests were carried out under UV-A light, but the real frontier will have to transform these materials active and efficient to sunlight and artificial light. The artificial lighting in the most part of the indoor environments is achieved with LED lamps, without any contribution of UV irradiation. Concerning this, many studies on the commercial micro-sized powders show that, modifying TiO_2, it is possible to make it photoactive even to the visible wavelengths [62, 63]. This is very promising for a future application on porcelain grés tiles and for their application in the indoor environments lit by LED lights.

3.3. Self-cleaning tests

The surface of the WGA sample is coated with a film of oleic acid (**Figure 19**), following the method described in the experimental section. In the presence of UV irradiation, this substance is completely degraded, proving that the substrate has photocatalytic properties. Measurement was carried out according to the mentioned ISO Standard, by monitoring the change of the contact angle of a drop of water that fell onto the sample surface, which was illuminated by a UV-A source at known wavelength and power.

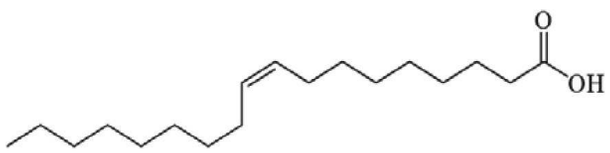

Figure 19. Oleic acid structure.

http://dx.doi.org/10.5772/62892

When between the beginning and the end of the test (76 hours), there is a variation in the contact angle, a photocatalytic material can be defined as *self-cleaning*.

The results of the measurements on WGA tiles are summarized in **Figure 20** that shows two pictures taken and processed by the instrument used for the contact angle measurements.

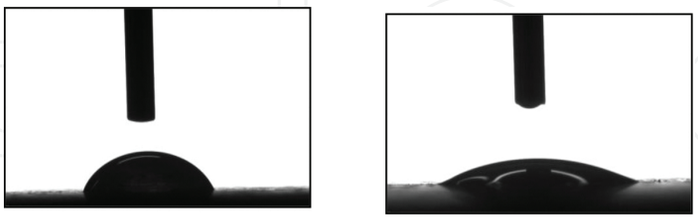

Figure 20. Profile of the water drops at time 0 (image on the left) and at 76 hours (image on the right) on a WGA slab.

Contact angle value of the WGA sample stored in the dark was also examined, but only at the end of the 76 hours. The comparison between the two tested slabs is listed in **Table 2**:

Sample	UV	Original slab contact angle	Contact angle t_0	Contact angle t_{48}	Contact angle t_{76}
WGA	Yes	31.3° ± 0.9°	68.5° ± 1.0°	41.0° ± 2.9°	30.1° ± 2.8°
WG A	No	31.3° ± 0.9°	67.8° ± 0.9°	—	68.2° ± 1.1°

Table 2. Summarizing data from self-cleaning test.

As shown in the table, the value of the contact angle gradually decreases from time t_0 to t_{76}, achieving the original value measured before the application of oleic acid onto the tile surface. This is due to the photocatalytic efficiency of the material, which is then able to degrade the oleic acid under UV irradiation [64].

The contact angle value at 72, 74 and 76 hours is constant, and it has returned to the value of the pristine ceramic surface at the beginning of the test, demonstrating that the oleic acid molecule has been completely degraded. On the contrary, there were no changes in the value of the contact angle of the sample of WGA treated with oleic acid but kept in the dark, confirming that natural degradation is not effective and that the photocatalytic process is needed to activate the photodegradation of the organic contaminant.

3.4. Test on antibacterial properties

Antibacterial tests performed on WGA samples confirmed the efficiency of the material to destroy bacteria present at the ceramic surface. Test results are reported in **Table 3**:

Experimental conditions of the test such as bacterial strains, temperature, humidity, irradiation, exposure time etc. are similar to the common condition of applications on the WGA. To evaluate the antibacterial activity of WGA, *E. coli* (Gram negative), as common inhabitant of human and animal intestine and therefore a suitable indicator of drinking water and quality

food, and *S. aureus* (Gram positive) as human pathogen bacteria in particular the MRSA strain, characterized by some antibiotic-resistance to beta-lactam, have been chosen.

Test	Unit Measurement	Results	
Antibacterial activity of photocatalytic materials—materials		***E. coli* ATCC 8739**	***Staphylococcus aureus* MRSA ATCC 43300**
No. of bacteria inoculated	Cells /ml	1,100,000	1,500,000
A—Average number of bacteria Non-treated specimens after inoculation	cells /ml	160,000	230,000
B_L—Average number of bacteria non -treated specimens after UV irradiation	cells /ml	170,000	108,000
C_L—Average number of bacteria photocatalytic treated specimens after UV irradiation	cells /ml	10	10
R_L—Photocatalytic antibacterial activity value after UV irradiation	Log10	4.2	4.0
Reductions of bacteria from non-treated specimens after UV irradiation	%	99,994	99,991
B_D—Average number of bacteria non-treated specimens after being kept in a dark place	cells /ml	600,000	400,000
C_D—Average number of bacteria photocatalytic treated specimens after being kept in a dark place	cells /ml	130,000	37,000
ΔR—Photocatalytic antibacterial activity value with UV irradiation	Log10	3.6	3.0

Table 3. Summary of the antibacterial results on WGA.

Test was performed at 25°C ± 1°C, temperature in the range of activity of the photocatalytic process and vitality of the microorganism tested both mesophilic. Test was conducted at pH 7.0 ± 0.2 (1/500 Nutrient broth), pH is an influential parameter for organism viability and a neutral pH near 7 is optimal for many biological processes. Test was performed in aerobic conditions (oxygen presence) to favour *E. coli* and *S. aureus* viability (aerobe/anaerobe facultative) at 0.25 $mWcm^{-2}$ as normally indoor exposure beside the window in the daytime, for 8 hours of exposure time.

The antibacterial tests in this work passed all the evaluation conditions as:

1. The logarithmic value of the number of viable bacteria of non-treated specimens after inoculation derived from the equation: $(L_{max}-L_{min})/(L_{mean}) \leq 0.2$, where L_{max} is the maximum logarithmic value of viable bacteria, L_{min} is the minimum logarithmic value of viable bacteria, L_{mean} is the average logarithmic value of viable bacteria for three specimens;

http://dx.doi.org/10.5772/62892

2. The logarithmic value of viable bacteria of non-treated specimens after inoculation shall be within the 1.0×10^5 to 4.0×10^5 cell range;

3. The viable bacteria of non-treated specimens after light exposure shall be more than 1.0×10^3 cells for all three specimens;

4. After being kept in a dark place, the viable bacteria of non-treated specimens shall be more than 1.0×10^3 cells for all three specimens.

In the first test, the average logarithmic value of *E. coli* for three non-treated specimens after inoculation is 160,000 cells/ml, and this value increases to 600,000 cells/ml after being kept in a dark place, and a 170,000 cells/ml after 8 hours of UV irradiation. The average logarithmic value of *E. coli* for three treated specimens decreases to 130,000 cells/ml after being kept in a dark place, and a 10 cells/ml after 8 hours of UV irradiation.

In the second test, the average logarithmic value of *S. aureus* for three non-treated specimens after inoculation is 230,000 cells/ml, and this value increases to 400,000 cells/ml after being kept in a dark place, and 108,000 cells/ml after 8 hours of UV irradiation. The average logarithmic value of irradiation.

For both bacterial strains, an increase after being kept in a dark place on non-treated specimens is observed, but greater for *E. coli* than *S. aureus*, and a decrease was observed for treated specimens, but greater for *S. aureus* than *E. coli*. These differences may be due to the different structures of the cell wall of the two bacterial strains, and bacterial reduction is imputable to non-photocatalytic antibacterial activity which can be present in different intensities in ceramic tiles. Both microorganisms tested same decrease after UV irradiation is detected and WGA showed a photocatalyst antibacterial activity R greater than 2 (reduction greater than 99.99%); the antibacterial activity is similar for both Gram negative and Gram positive bacteria, including strains with methicillin resistance.

These results indicate that the action of reactive oxygen species (ROS), generated during the photocatalysis, on cell wall, cell membrane and internal cellular components, is very effective, and it does not seem to be affected by methicillin-resistant mechanisms. The same trend is observed for ΔR (photocatalyst antibacterial activity value with UV irradiation); the values obtained for *E. coli* and *S. aureus* (3.6 and 3.0) indicate a good photoefficiency on the WGA tiles.

4. Conclusions

Micro-sized TiO_2 can successfully replace the nanometric powders for photocatalytic applications, as well as for the removal of dirt or bacteria from surfaces. The use of micrometric powders of TiO_2 brings several advantages in terms of health safety, limitation of the problems related to the use of nano-powders in industries and cost.

From a chemical point of view, the commercial and micro-sized sample K1077 consists completely of anatase, which is the most photoactive crystallographic phase, as well as it exhibits a rather high population of hydroxyl radicals at the surface that confer an improve-

ment of the performances in terms of pollutant oxidation. From an economic point of view, micro-TiO_2 is much cheaper than the commercial nano-powders. In particular for high amount of powder, the replacement of the nano-powder by micro-powder leads to an extremely high cost saving. Moreover, micrometric TiO_2 is overall efficient against all the different pollutants, with a not so high difference in performance compared to nano-TiO_2, especially in pollution levels closest to the actual values.

The application of micro-TiO_2 on porcelain grés tiles paves the way to a new scenario of products to improve the quality of life. Indeed, when TiO_2 is coated on the porcelain grés tiles, all its properties can be fully exploited. Not only the photocatalytic tiles show self-cleaning features and antibacterial properties, but also they are able to degrade both organic and inorganic pollutants in gas and liquid phases. Particularly, the possibility to exploit the photocatalytic properties of tiles even in aqueous phase is a real innovation compared with most of the photocatalytic building materials, already available in the market.

To conclude, the use of micro-TiO_2 is an actionable and necessary road, as well as the photocatalytic tiles coated with micro-powders are actually effective for a real improvement of our indoor and outdoor environments.

Acknowledgements

The work was partially financed by the project "Azione A del Dipartimento di Chimica per il Piano di Sostegno alla Ricerca – 2015/2017 - Linea 2" by the Dipartimento di Chimica, Università degli Studi di Milano.

Author details

Claudia L. Bianchi[1*], Carlo Pirola[1], Marta Stucchi[1], Benedetta Sacchi[1], Giuseppina Cerrato[2], Sara Morandi[2], Alessandro Di Michele[3], Alessandra Carletti[4] and Valentino Capucci[5]

*Address all correspondence to: claudia.bianchi@unimi.it

1 University of Milan – Department of Chemistry, Milan, Italy

2 University of Turin – Department of Chemistry, Turin, Italy

3 University of Perugia – Department of Physics and Geology, Perugia, Italy

4 Artest SpA, Modena, Italy

5 GranitiFiandre Group, Castellarano, Italy

References

[1] Macwan D.P., Dave P.N., Chaturvedi S. (2011). A review on nano-TiO_2 sol–gel tyspe syntheses and its applications. *Material Science*, Vol. 46, pp. 3669–3686.

[2] Ismail A.A., Bahnemann D.W. (2011). Mesoporous titania photocatalysts: preparation, characterization and reaction mechanisms. *Journal of Materials Chemistry*, Vol. 21, pp. 11686.

[3] Fujishima A., Honda K. (1972). Electrochemical photolysis of water at a semiconductor electrode. *Nature*, Vol. 238, pp. 37–38.

[4] Rios P.F., Dodiuk H., Kenig S., McCarthy S., Dotan A. (2007). The effect of polymer surface on the wetting and adhesion of liquid systems. *Adhesion Science Technology*, Vol. 21, pp. 227–241.

[5] Kaune G., Memesa M., Meier R., Ruderer M.A., Diethert A., Roth S.V., D'Acunzi M., Gutmann J.S., Mueller-Buschbaum P. (2009). Hierarchically structured titania films prepared by polymer/colloidal templating. *ACS Applied Materials & Interfaces*, Vol. 1, pp. 2862–2869.

[6] Morris, A.J., Meyer, G.J. (2008). TiO_2 surface functionalization to control the density of states. *Journal of Physical Chemistry C*, Vol. 112, pp. 18224–18231.

[7] Kumar S.G., Devi L.G. (2011). Review on modified TiO_2 photocatalysis under UV/visible light: selected results and related mechanisms on interfacial charge carrier transfer dynamics. *The Journal of physical chemistry A*, Vol. 115 No. 46, pp. 13211–13241.

[8] Lawless D., Serpone N., Meisel D. (1991). Role of OH radicals and trapped holes in photocatalysis. A pulse radiolysls study. *Journal of Physical Chemistry*, Vol. 95, pp. 5166–5170.

[9] Mineral Commodity Summaries (2011). Titanium and titanium dioxide. U.S. *Geological Survey*, Retrieved from http://minerals.usgs.gov/minerals/pubs/mcs/2011/mcs2011.pdf

[10] Bianchi C.L., Pirola C., Galli F., Cerrato G., Morandi S., Capucci V. (2014). Pigmentary TiO_2: a challenge for its use as photocatalyst in NOx air purification. *Chemical Engineering Journal*, Vol. 261, pp. 76–82.

[11] Patil S.S., Shedbalkar U.U., Truskewycz A., Chopaded B.A., Ball A.S. (2016). Nanoparticles for environmental clean-up: a review of potential risks and emerging solutions. *Environmental Technology & Innovation*, Vol. 5, pp. 10–21.

[12] Wang J., Gerlach J.D., Savage N., Cobb G.P. (2013). Necessity and approach to integrated nanomaterial legislation and governance. *Science of the Total Environment*, Vol. 442, pp. 56–62.

[13] Alivisatos A. P. (1996). Perspectives on the physical chemistry of semiconductor nanocrystals. *Journal of Physical Chemistry*, Vol. 100, pp. 13226.

[14] Vishwakarma V., Samal S.S., Manoharan N. (2010). Safety and risk associated with nanoparticles - a review. *Journal of Minerals & Materials Characterization & Engineering*, Vol. 9, No. 5, pp. 455–459.

[15] Bermudez E., Mangum J., Wong B., Asgharian B., Hext P., Warheit D., et al. (2004). Pulmonary responses of mice, rats, and hamsters to subchronic inhalation of ultrafine titanium dioxide particles. *Toxicological Sciences*, Vol. 77, pp. 347–357.

[16] Oberdörster G., Oberdörster E., Oberdörster J. (2005). Nanotoxicology: an emerging discipline evolving from studies of ultrafine particles. *Environmental Health Perspectives*, Vol. 113, No.7, pp. 823–839.

[17] Sharma N., Kalra K.L., Oberoi H.S., Bansal S. (2007). Optimization of fermentation parameters for production of ethanol from kinnow waste and banana peels by simultaneous saccharification and fermentation. *Indian Journal of Microbiology*, Vol. 47, No.4, pp. 310–316.

[18] Sayes C.M., Gobin A.M., Ausman K.D., Mendez J., West J.L., Colvin V.L. (2005). Nano-C60 cytotoxicity is due to lipid peroxidation. *Biomaterials*, Vol. 26, No. 36, pp. 7587–7595.

[19] Silva F., Arezes P., Swuste P. (2015). Risk assessment in a research laboratory during sol–gel synthesis of nano-TiO_2. *Safety Science*, Vol. 80, pp. 201–212.

[20] Review of Human Carcinogens. IARC Monographs, vol. 100, Retrieved from http://monographs.iarc.fr

[21] NIOSH, The national institute for occupational safety and health, Retrieved from www.cdc.gov/niosh

[22] Heinrich U., Fuhst R., Rittinghausen S., Creutzenberg O., Bellmann B., Koch W., Levsen K. (1995). Chronic inhalation exposure of Wistar rats and two different strains of mice to diesel engine exhaust, carbon black, and titanium dioxide. *Inhalation Toxicology: International Forum for Respiratory*, Vol. 7, No. 4, pp. 533–556.

[23] Bianchi C.L., Pirola C., Gatto S., Nucci S., Minguzzi A., Cerrato G., Biella S., Capucci V. (2012). New surface properties in porcelain grés tiles with a look to human and environmental safety. *Advances in Materials Science and Engineering*, Vol. 2012, 8 p.

[24] Bianchi C.L., Gatto S., Pirola C., Scavini M., Vitali S., Capucci V. (2013). Micro-TiO_2 as a starting material for new photocatalytic tiles. *Cement and Concrete Composites*, Vol. 36, pp. 116–120.

[25] Bianchi C.L., Gatto S., Pirola C., Naldoni A., Di Michele A., Cerrato G., Crocellà V., Capucci V. (2014). Photocatalytic degradation of acetone, acetaldehyde and toluene in gas-phase: comparison between nano and micro-sized TiO_2. *Applied Catalysis B: Environmental*, Vol. 146, pp. 123–130.

[26] Taurino R., Barbieri L., Bondioli F. (2016). Surface properties of new green building material after TiO_2–SiO_2 coatings deposition. *Ceramics International*, Vol. 42, pp. 4866–4874.

[27] Graziani L., Quagliarini E., Bondioli F., D'Orazio M. (2014). Durability of self-cleaning TiO_2 coatings on fired clay brick facades: effects of UV exposure and wet & dry cycles. *Building and Environment*, Vol. 71, pp. 193–203.

[28] Chen J., Poon C.S. (2009). Photocatalytic construction and building materials: from fundamentals to applications. *Building and Environment*, Vol. 44, pp. 1899–1906.

[29] Zhao J., Yang X.D. (2003). Photocatalytic oxidation for indoor air purification: a literature review. *Building Environment*, Vol. 38, pp. 645–654.

[30] Diamanti M.V., Del Curto B., Ormellese M., Pedeferri M.P. (2013). Photo-catalytic and self-cleaning activity of colored mortars containing TiO_2. *Construction and Building Materials*, Vol.46, pp. 167–174.

[31] Sciancalepore C., Bondioli F. (2015). Durability of SiO_2–TiO_2 photocatalytic coatings on ceramic tiles. *International Journal of Applied Ceramic Technology*, Vol. 12, pp. 679–684.

[32] Zhao X.J., Zhao Q.N., Yu J.G., Liu B.S. (2008). Development of multifunctional photoactive self-cleaning glasses. *Journal of Non-Crystal Solids*, Vol. 354, pp. 1424–1430.

[33] Quagliarini E., Bondioli F., Goffredo G.B., Licciulli A., Munafo P. (2012). Smart surfaces for architectural heritage: preliminary results about the application of TiO_2-based coatings on travertine. *Journal of Cultural Heritage*, Vol. 13, pp. 204–209.

[34] Casasola R., Rinco'n J. M., Romero M. (2012). Glass-ceramic glazes for ceramic tiles: a review. *Journal of Materials Science*, Vol. 47, No. 2, pp. 553–582.

[35] Bianchi C.L., Gatto S., Nucci S., Cerrato G., Capucci V. (2013). Self-cleaning measurements on tiles manufactured with micro-sized photoactive TiO_2. *Advances in Materials Research, An Interntional Journal*, Vol. 2, No. 1, pp. 65–75.

[36] Ragesh P., Ganesh V.A., Naira S.V. (2014). A review on self-cleaning and multifunctional materials. *Materials Chemistry A*, Vol. 2, pp. 14773.

[37] Furstner R., Barthlott W., Neinhuis C., Walzel P. (2005). Wetting and self-cleaning properties of artificial superhydrophobic surfaces. *Langmuir*, Vol. 21, pp. 956–961.

[38] Cappelletti G., Fermo P., Camiloni M. (2015). Smart hybrid coatings for natural stones conservation. *Progress in Organic Coatings*, Vol. 78, pp. 511–516.

[39] La Russa M.F., Ruffolo S.A., Rovella N., Belfiore C.M., Palermo A.M., Guzzi M.T., Crisci G.M. (2012). Multifunctional TiO_2 coatings for cultural heritage. *Progress in Organic Coatings*, Vol. 74, pp. 186–191.

[40] Quagliarini E., Bondioli F., Goffredo G.B., Cordoni C., Munafò P. (2012). Self-cleaning and de-polluting stone surfaces: TiO_2 nanoparticles for limestone. *Construction and Building Materials*, Vol. 37, pp. 51–57.

[41] Manoudis P.N., Tsakalof A., Karapanagiotis I., Zuburtikudis I., Panayiotou C. (2009). Fabrication of super-hydrophobic surfaces for enhanced stone protection. *Surface and Coatings Technology*, Vol. 203, pp. 1322–1328.

[42] Matsunaga T., Tomoda T., Nakajima T., Wake H. (1985). Photoelectrochemical sterilization of microbial cells by semiconductor powders. *FEMS Microbiology Letters*, Vol. 29, pp. 211–214.

[43] Scuderi V., Buccheri M.A., Impellizzeri G., Di Mauro A., Rappazzo G., Bergum K., Svensson B.G., Privitera V. (2016). Photocatalytic and antibacterial properties of titanium dioxide flat film. *Materials Science in Semiconductor Processing*, Vol. 42, pp. 32–35.

[44] Fostera H.A., Sheel D.W., Sheel P., Evans P., Varghese S., Rutschke N., Yates H.M. (2010). Antimicrobial activity of titania/silver and titania/copper films prepared by CVD. *Journal of Photochemistry and Photobiology A: Chemistry*, Vol. 216, No. 2-3, pp. 283–289.

[45] Bianchi C.L., Pirola C., Galli F., Vitali S., Minguzzi A., Stucchi M., Manenti F., Capucci V. (2016). NO_x degradation in a continuous large-scale reactor using full-size industrial photocatalytic tiles. *Catalysis Science & Technology*, DOI: 10.1039/C5CY01627D.

[46] Bianchi C.L., Colombo E., Gatto S., Stucchi M., Cerrato G., Morandi S., Capucci V. (2014). Photocatalytic degradation of dyes in water with micro-sized TiO_2 as powder or coated on porcelain-grès tiles. *Journal of Photochemistry and Photobiology A: Chemistry*, Vol. 280, pp. 27–31.

[47] Foster G., Annan J.D., Jones P.D., Mann M.E., Mullan B., Renwick J., Salinger J., Schmidt G.A., Trenberth K.E. (2010). Comment on Influence of the Southern Oscillation on tropospheric temperature by J.D. McLean, C.R. de Freitas, and R.M. Carter. *Journal of Geophysical Research*, Vol. 115, pp. 1-4.

[48] Ardizzone S., Bianchi C.L., Cappelletti G. (2006). Growth of TiO_2 nanocrystals in the presence of alkylpyridinium salts: the interplay between hydrophobic and hydrophilic interactions. *Surface and Interface Analysis*, Vol. 38, No. 4, pp. 452–457.

[49] Ardizzone S., Bianchi C.L., Cappelletti G., Gialanella S., Pirola C., Ragaini V. (2007). Tailored anatase/brookite nanocrystalline TiO_2. The optimal particle features for liquid and gas-phase photocatalytic reactions. *Journal of Physical Chemistry C*, Vol. 111, No. 35, pp. 13222–13231.

[50] Ardizzone S., Bianchi C.L., Cappelletti G., Naldoni A., Pirola C. (2008). Photocatalytic degradation of toluene in the gas phase: relationship between surface species and catalyst features. *Environmental Science & Technology*, Vol. 42, No.17, pp. 6671–6676.

[51] Naldoni A., Bianchi C.L., Pirola C., Suslick K.S. (2013). TiO_2 porous microsphere with tunable properties for air purification. *Ultrasonics Sonochemistry*, Vol. 20, pp. 445–451.

[52] Naldoni A., Allieta M., Santangelo S., Marelli M., Fabbri F., Cappelli S., Bianchi C.L., Psaro R., Dal Santo V. (2012). Effect of nature and location of defects on bandgap narrowing in black TiO_2 nanoparticles. *Journal of the American Chemical Society*, Vol. 134, pp. 7600–7603.

[53] Chen X., Burda C. (2008). The electronic origin of the visible-light absorption properties of C-, N-and S-doped TiO_2 nanomaterials. *Journal of the American Chemical Society*, Vol. 130, pp. 5018–5019.

[54] ASTM C373-88 (2006). Standard test method for water absorption, bulk density, apparent porosity, and apparent specific gravity of fired whiteware products. *ASTM International*, Retrieved from http://www.astm.org/DATABASE.CART/HISTORICAL/C373-88R06.htm.

[55] ISO 10545-7 (1996). Ceramic tiles, Part 7: determination of resistance to surface abrasion for glazed tiles. Retrieved from http://www.iso.org/iso/catalogue_detail.htm

[56] ISO 10545-12 (1995). Ceramic tiles, Part 12: determination of frost resistance. Retrieved from http://www.iso.org/iso/iso_catalogue/catalogue_tc/catalogue_detail.htm

[57] Anderson C., Bard A.J. (1997). Improved photocatalytic activity and characterization of mixed TiO_2 /SiO_2 and TiO_2/Al_2O3 materials. *Journal of Physical Chemistry B*, Vol. 101, No. 14, pp. 2611–2616.

[58] Xie T.H., Lin J. (2007). Origin of photocatalytic deactivation of TiO2 film coated on ceramic substrate. *Journal of Physical Chemistry C*, Vol. 111, No. 27, pp. 9968–9974.

[59] Wang R., Hashimoto K., Fujishima A. (1997). Light-induced amphiphilic surfaces. *Nature*, Vol. 388, No. 6641, pp. 431–432.

[60] Cerrato G., Bianchi C.L., Morandi S., Pirola C., Stucchi M., Diamanti M.V., Pedeferri M.P., Capucci V. (2015). The role of nano/microstructure in the case of the photodegradation of two model VOC pollutants using commericial TiO_2. *Energy and Environment Focus*, Vol. 4, pp. 226–231.

[61] Bianchi C.L., Pirola C., Galli F., Stucchi M., Morandi S., Cerrato G., Capucci V. (2015). Nano or micro- TiO_2 for the photodegradation of ethanol: experimental data and kinetic modeling. *RSC Advances*, Vol. 5, pp. 53419–53425.

[62] Stucchi M., Bianchi C.L., Pirola C., Vitali S., Cerrato G., Morandi S., Argirusis C., Sourkouni G., Sakkas P.M., Capucci V. (2015). Surface decoration of commercial micro-sized TiO_2 by means of high energy ultrasound: a way to enhance its photocatalytic activity under visible light. *Applied Catalysis B, Environmental*, Vol. 178, pp. 124–132.

[63] Stucchi M., Bianchi C.L., Pirola C., Cerrato G., Morandi S., Argirusis C., Sourkouni G., Naldoni A., Capucci V. (2016). Copper NPs decorated titania: a novel synthesis by high

energy US with a study of the photocatalytic activity under visible light. *Ultrasonics Sonochemistry*, Vol. 31, pp. 295–301.

[64] Watanabe T., Fukayama S., Miyauchi M., Fujishima A., Hashimoto K. (2000). Photocatalytic activity and photo-induced wettability conversion of TiO_2 thin film prepared by sol-gel process on a soda-lime glass. *Journal of Sol-Gel Science and Technology*, Vol. 19, No. 1–3, pp. 71–76.